Influence of the rupture initiation on the intersonic transition: Crack-like versus pulse-like modes

G. Festa[1] and J.-P. Vilotte[1]

Received 19 April 2006; revised 7 July 2006; accepted 11 July 2006; published 12 August 2006.

[1] We numerically investigate the supershear transition of inplane rupture under slip weakening friction and tectonic loading, using a non-smooth spectral element method. Nucleation of the rupture in the vicinity of an initial stress concentration is consistently solved together with the dynamic propagation. Nucleation is shown to influence the transition to the supershear propagation and, depending upon the initiation process and the level of the stress out of the nucleating asperity, crack-like or pulse-like solutions can be selected in the intersonic regime. Pulses are triggered by dynamic unloading of the traction ahead of the Rayleigh wave and tend to become metastable. The asymptotic numerical solution is always a crack propagating close to P wave speed. The rupture front and the arrest velocities are numerically characterized. We argue that the nucleation phase introduces a trade-off with the state of the stress, in determining the distance at which supershear appears. **Citation:** Festa, G., and J.-P. Vilotte (2006), Influence of the rupture initiation on the intersonic transition: Crack-like versus pulse-like modes, *Geophys. Res. Lett.*, *33*, L15320, doi:10.1029/2006GL026378.

1. Introduction

[2] An increasing number of observations are supporting supershear propagation, for example, rupture speeds between the shear (c_s) and the dilatational (c_p) wave velocities, during some strike-slip earthquakes [*Bouchon and Vallée*, 2003; *Dunham and Archuleta*, 2004] and at the scale of laboratory experiments, under far-field loading and local explosive triggering [*Xia et al.*, 2004].

[3] In the limit of the singular elastodynamics, admissible speeds v for steady-state propagation are shown to exist in both sub-Rayleigh and intersonic domains [*Freund*, 1979; *Broberg*, 1999]. While in the sub-Rayleigh range the stress is square-root singular with the energy release rate G decreasing to zero as $v \rightarrow c_r$, in the intersonic regime the tip singularity is always smaller than 1/2 except at the Eshelby speed $\sqrt{2}c_s$, where Mach waves disappear.

[4] When using cohesive models [*Broberg*, 1999], for a self-similar shear crack expansion under uniform remote loading, G remains finite and non negative in the intersonic regime. If the size of the process zone is fixed, G increases from zero at $v = c_s$ to a maximum value at $v \approx \sqrt{2}c_s$ and then decreases to zero as $v \rightarrow c_p$. On the other hand, for a fixed fracture energy G_c, the intersonic speed is selected by a dynamic energy balance and tends asymptotically to c_p. By perturbation analysis, steady-state propagation is found to be stable between 1.33 c_s and c_p [*Obrezanova and Willis*, 2003].

[5] Analytical studies of transient expansion of self-similar shear cracks, in the limit of zero cohesive zone [*Burridge*, 1973], indicate a shear-stress peak ahead of the main rupture, which may trigger a secondary rupture. When supershear occurs, the rupture always accelerates toward c_p. This transition mechanism was numerically confirmed by *Andrews* [1976] in the case of slip weakening friction and spontaneous crack initiation.

[6] Recently, nucleation and dynamic propagation of shear-rupture were shown to depend on finer details of the friction. In the limit of linear slip weakening, the rupture nucleation in the region of an initial stress concentration is characterized by a stable expansion, until a universal critical size is reached. Then, an unstable dynamic phase emerges with an exponential acceleration of slip [*Campillo and Ionescu*, 1997; *Ampuero et al.*, 2002; *Uenishi and Rice*, 2003]. Large scale yielding is likely to occur during the nucleation, that is, energy is dissipated over the whole slipping patch, in contrast to small scale yielding during crack propagation, where energy dissipation is confined at the crack tip within a finite process zone, which decreases as the rupture speed increases. An other issue is related to the mode of rupture propagation. Analytical and numerical investigations [*Broberg*, 1978; *Nielsen and Madariaga*, 2003], point out the existence of pulse solutions for shear-rupture propagation, when frictional strength can be rapidly recovered after the onset of healing.

[7] In the light of these results, we numerically investigate intersonic solutions for inplane shear rupture using a non-smooth spectral element method. Special attention is devoted to the nucleation phase in the selection of pulse-like or crack-like solutions.

2. Numerical Technique

[8] In-plane rupture initiation and propagation along similar interfaces, held by slip weakening friction, is numerically investigated using the spectral element method (SEM) [*Komatitsch and Vilotte*, 1998]. To account for discontinuities of kinematic fields across the fault, the elastic domain Ω is split into two non-overlapping regions Ω^I and Ω^{II}, such that the fault Γ is located on the common boundary. When gathering information from both domains, the weak elastodynamic formulation yields:

$$\int_{\Omega} \rho \mathbf{w} \dot{\mathbf{v}} d\Omega = -\int_{\Omega} \nabla \mathbf{w} : \boldsymbol{\sigma} d\Omega + \int_{\Gamma} \delta \mathbf{w} \mathbf{T} d\Gamma \qquad (1)$$

[1]Seismology Laboratory, Institut de Physique du Globe de Paris, Paris, France.

0094-8276/06/2006GL026378

where ρ is the density, $\mathbf{v} = (\mathbf{v}^I, \mathbf{v}^{II})$ is the velocity, $\boldsymbol{\sigma} = (\boldsymbol{\sigma}^I, \boldsymbol{\sigma}^{II})$ the stress, $\mathbf{w} = (\mathbf{w}^I, \mathbf{w}^{II})$ an admissible displacement perturbation and $\delta\mathbf{w}$ an admissible slip perturbation across Γ. Conditions on the fault are expressed as non-smooth relations between the traction $\mathbf{T}$ acting on it, the slip $\delta\mathbf{u} = \mathbf{u}^{II}|_\Gamma - \mathbf{u}^I|_\Gamma$, and the slip rate $\delta\mathbf{v}$. After discretization of the elastic medium and the fault interface, projection of the kinematic fields onto local polynomial basis and numerical quadrature lead to a linear algebraic system:

$$\mathbf{M}\mathbf{v}_{n+1} = \mathbf{M}\mathbf{v}_n + \Delta t\left(\mathbf{F}^{int} + \mathbf{B}^T\mathbf{T}\right)_{n+1/2} \tag{2}$$

where $\mathbf{F}^{int}$ is the internal forces contribution, $\mathbf{B}^T$ an interface matrix and subscripts refer to time discretization. With explicit time stepping, diagonality of the mass matrix $\mathbf{M}$ allows for efficient wave propagation solvers. In the following, the fault discretization is inherited by a conforming discretization of Ω^I and Ω^{II}. Condensation of equation (2) onto the fault interface leads to a discrete linear impedance, relating slip rate and traction:

$$\delta\mathbf{v}_{n+1} = \delta\mathbf{v}^{free} + \Delta t\left[1/2\mathbf{H}\mathbf{M}^{-1}\mathbf{B}^T\right]\mathbf{T}_{n+1} \tag{3}$$

where

$$\delta\mathbf{v}^{free} = \delta\mathbf{v}_n + \Delta t\mathbf{H}\mathbf{M}^{-1}\left[\mathbf{F}^{int}_{n+1/2} + (1/2)\mathbf{B}^T\mathbf{T}_n\right] \tag{4}$$

and $\mathbf{H}$ the condensation matrix. Equation (3) has to be solved under contact and friction constrains to determine the actual traction on the fault. Non-smooth Signorini law and slip weakening, expressed as state-dependent Coulomb friction, are here implicitly solved [*Jean*, 1999]. Spurious high-frequency standing waves are eliminated by introducing a complex prolongation in the direction normal to the fault, resulting in a causal filter [*Festa and Vilotte*, 2005].

3. Transition to the Supershear

[9] We consider the inplane crack problem along a preexisting straight interface between two homogeneous elastic half-spaces. Linear slip weakening friction [*Ida*, 1972] is assumed with a strength threshold τ_u. Once the shear traction on the interface reaches that threshold, slip may occur. Afterward, the frictional strength of the interface depends on the slip history and drops to a dynamic value τ_f over a characteristic distance D_c, with constant slip weakening rate $\gamma = (\tau_u - \tau_f)/D_c$.

[10] Rupture is nucleated in a region of initial stress concentration. We impose the quasi-static solution of *Uenishi and Rice* [2003] as initial condition to consistently solve the unstable dynamic nucleation and the rupture propagation via the spectral element method. Following *Uenishi and Rice* [2003], a Gaussian shaped initial traction $\tau_i(x) = \tau_u - \alpha a^2(1 - e^{x^2/2a^2})$ (x the distance along the interface, a the characteristic length of the stress asperity, α a constant to be defined), is increased by a uniform loading at a constant rate. At the onset of the instability, the size of the slipping patch is $l_c = \xi\frac{\mu^{eq}}{\gamma}$, where $\xi \approx 1.158$ is independent of the initial profile of traction and $\mu^{eq} = \mu/(1 - \nu)$ with ν the Poisson ratio.

[11] The profile of the slip over l_c is computed by a Chebyshev expansion of the solution and the corresponding traction τ_0 by Hilbert transform. Finally, the constant α is chosen by imposing a prescribed value τ_0^* far from the critical slipping patch and it also accounts for the load increase during the metastable nucleation. It is worth to note that different results would be obtained if the nucleation is bypassed using a prescribed initial stress drop over a finite region of the interface.

[12] The dynamic rupture simulations can be analyzed in terms of two non-dimensional parameters. The s parameter

$$s = \frac{\tau_u - \tau_0^*}{\tau_0^* - \tau_f} \tag{5}$$

measures the actual fault strength with respect to the released stress, this is, dynamic stress drop $\Delta\tau = \tau_0^* - \tau_f$. For a linear slip weakening friction and stress drop rupture, *Andrews* [1985] estimated that supershear always occurs when $s < 1.77$. The second parameter a/l_c is related to the nucleation process, that is, the width of the Gaussian asperity over the critical nucleation length, and can be associated with the parameter $\kappa = \frac{\Delta U}{G_c} = f(\frac{a}{l_c})$ [*Madariaga and Olsen*, 2000], if restricted to the critical slipping patch (ΔU is the available elastic strain energy rate and $G_c = \frac{1}{2}(\tau_u - \tau_f)D_c$ the fracture energy). The simulations have been performed with non-dimensional parameters ($\mu = 1$, $c_s = 1$, $\gamma = 1$, and $D_c = 1.8$) and 15 to 30 points per l_c.

[13] First, we consider rupture propagation for $s = 0.8$ and $a/l_c = 1$. In Figure 1 the normalized shear traction (solid line) and slip rate (dashed line) are plotted at the onset of the supershear regime and after the generation of the pulse. The traction is normalized as $(\tau - \tau_0^*)/\Delta\tau$ and the slip rate as $\delta\nu\mu^{eq}/c_s\Delta\tau$. On the same figure, the vorticity of the velocity field in the medium, enhancing shear motion, is shown. The dynamic nucleation is slow with a weak increase of the size of the nucleation patch during the exponential slip growth at the center. After the onset of the rupture, the crack front accelerates to the Rayleigh speed (Figure 1a, R) with a large amount of radiated shear energy sent ahead of it. It propagates at about c_s speed (Figure 1c), building up a peak in the traction (Figure 1a, S) that triggers a forward rupture with its own nucleation. After the coalescence of the two cracks, the process zone shrinks as the rupture speed tends to c_p (Figure 1b, P). A forward pulse is now generated with an arrest phase moving at a constant velocity $\approx 0.95\ c_s$. It corresponds to an unloading of the traction below the dynamic strength threshold (Figure 1b, S). The supershear transition occurs after a traveling distance $L/l_c = 20.7$.

[14] When increasing a/l_c to 2, the stress distribution becomes broader and the stress level is increased over some distance a. The dynamic nucleation phase is much faster and the solution drastically changes (Figure 2). When the rupture front reaches the Rayleigh wave speed, the amount of shear energy sent forward is now large enough to spontaneously generate the supershear. The traction bends forward (Figure 2a, sS) and the crack quickly accelerates to c_p (Figure 2b, P). The final shape of the slip rate profile remains crack-like, with a supershear front always connected to the Rayleigh interface wave (Figure 2b, R), the latter propagating without any additional dissipation. In

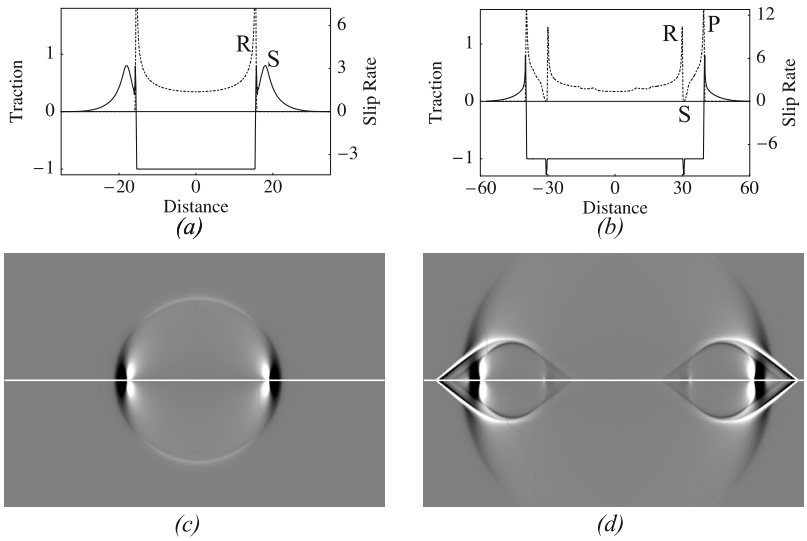

Figure 1. Slip rate (dotted line) and tangential traction (solid line) (a) at the beginning of the supershear and (b) after the pulse generation. (c–d) Snapshots of vorticity at the same times. Simulations have been run for $s = 0.8$ and $a/l_c = 1$. The shear energy sent ahead of the front (Figure 1c) generates a S peak in the traction (Figure 1a), that triggers the supershear rupture. The supershear solution (Figure 1b) is a pulse acceleration to c_p (P) with an arrest phase (S) in the slip rate corresponding to an unloading in the traction. The tip ultimately radiates Mach waves (Figure 1d), with the signature of the secondary nucleation observable behind them.

this case, the distance at which the supershear transition takes place is reduced to $L/l_c = 10.85$.

[15] In Figure 3, accelerations, recorded at a receiver located beyond the supershear transition, are compared for both regimes. In both cases, the largest amplitudes are carried out by the Mach shear waves (Sh) (Figures 1d and 2d), with a polarization at $\approx 30^o$ with respect to the fault, corresponding to a front propagating at c_p. While the nucleation P-wave (Pn) is observable for both cases, a secondary P-wave (Psn), associated with the supershear transition is clearly seen in the pulse-like solution. The Rayleigh wave is instead localized on the fault (Figures 1d and 2d) with a weak amplitude at the receiver, diminishing the hope of identifying a signature of the arrest.

[16] We explored the supershear behavior spanning s from 0.4 to 1.8, and a/l_c from 0.5 to 3. The corresponding phase diagram is shown in Figure 4 where the transition between pulse-like and crack-like regimes is drawn. This

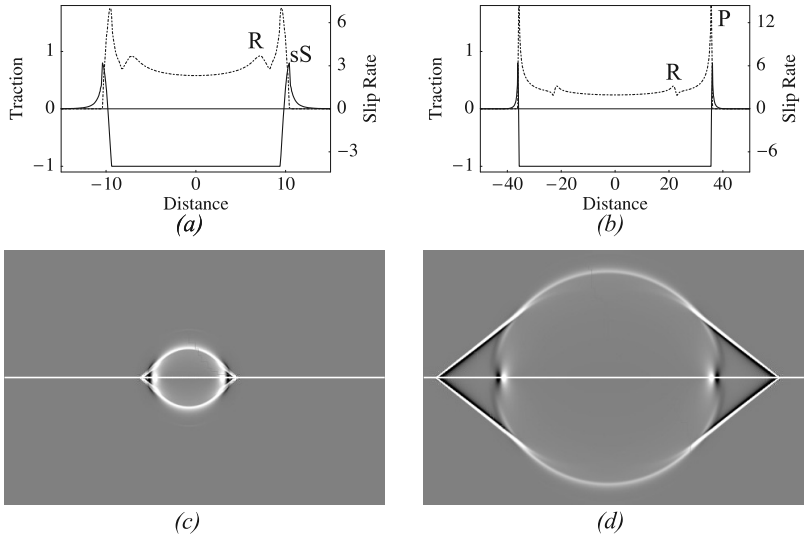

Figure 2. Slip rate (dotted line) and tangential traction (solid line) (a) at the beginning of the supershear and (b) at the steady propagation. (c–d) Snapshots of vorticity at the same times. Simulations have been run for $s = 0.8$ and $a/l_c = 2$. A large amount of shear energy at the onset of the rupture (Figure 2c) is able to spontaneously trigger the supershear, with a bending of the traction (Figure 2a) ahead of the Rayleigh front (R). The final solution (Figure 2b) is a crack, with the tip (P) always connected to the Rayleigh wave (R). The steady rupture mainly radiates shear Mach waves (Figure 2d), with a Rayleigh wave drastically reduced, as compared to Figure 1d.

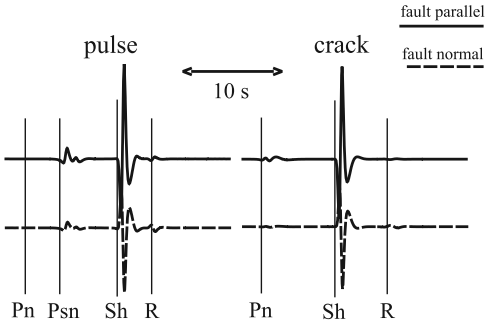

Figure 3. Accelerograms for the pulse-like and crack-like solutions are compared (Pn is P from nucleation, Psn is P from supershear nucleation, Sh is Mach wave and R Rayleigh wave). The largest amplitudes are carried out by the shear Mach waves, and the only difference is observable through the presence of a secondary nucleation phase Psn in the case of the pulse-like regime.

passage can be mapped as a non trivial function of a/l_c and s. Transition occurs for lower s values as a/l_c decreases. For $s \leq 0.6$, no pulse solution is observed: whatever a/l_c is, supershear always propagates as a connected crack. On the contrary for $s \geq 1.4$, the solution always exhibits a pulse. Superimposed on the figure, the graded gray scale indicates the distance L/l_c, measured from initial asperity center, at which the crack accelerates beyond c_s. Even though qualitative at this stage, such a parameter analysis points out the influence of the large-to-small scale yielding transition on the supershear generation. L/l_c happens to be a function not only of s, as pointed out by *Andrews* [1985], but also of the nucleation phase through a/l_c. Therefore the distance at which supershear transition occurs can be quite different for the same s value, depending on the nucleation, as large as one order of magnitude. Finally, the critical $s = 1.77$ [*Andrews*, 1985], above which only Rayleigh-wave speed is achievable, is also retrieved. Beyond $s = 1.8$, the traction peak sustained by the shear energy radiated ahead of the crack front is no longer able to reach the threshold.

[17] For $s = 0.8$ and $a/l_c = 1$, the shapes of the pulse at different stages of the propagation can be renormalized onto a single master curve using a t/x transformation. This is identified here as the signature of local self-similar geometry. The master shape is shown Figure 5a. The behavior of the slip rate in the vicinity of the tip is investigated on a log-log plot as a function of the distance from the tip (Figure 5b). A square-root divergence is found behind the tip in contrast with the analytical solution of *Burridge* [1973]. The same behavior is observed for crack-like solutions. The slip rate exhibits a logarithmic scaling in the vicinity of the healing. Pulse-like solutions are triggered by a dynamic unloading of the shear traction ahead of the Rayleigh wave below the frictional threshold, within a localized zone. During the evolution the healing zone spreads out and the amount of the unloading continuously decreases. Hence, pulse solutions can only be observed for a transient time before they become metastable and can be destabilized by small transient perturbations.

4. Conclusions

[18] We numerically show that the nucleation process and the large-to-small scale yielding transition need to be considered in the supershear transition mechanism. In the case of inplane cracks along preexisting straight interfaces, under slip weakening friction and tectonic loading, the dynamic rupture regimes can be analyzed in a phase diagram, defined in terms of two non-dimensional parameters. As a function of the relative strength excess s and a nucleation parameter a/l_c, defined as the ratio between the characteristic length of the initial stress concentration a and the critical nucleation size l_c, two regimes of supershear propagation are found.

[19] Intersonic pulses are observed for relatively large s and small a/l_c with a delayed supershear transition associated with a triggering mechanism ahead of the Rayleigh front, by the S-wave peak in the traction. Pulses can be

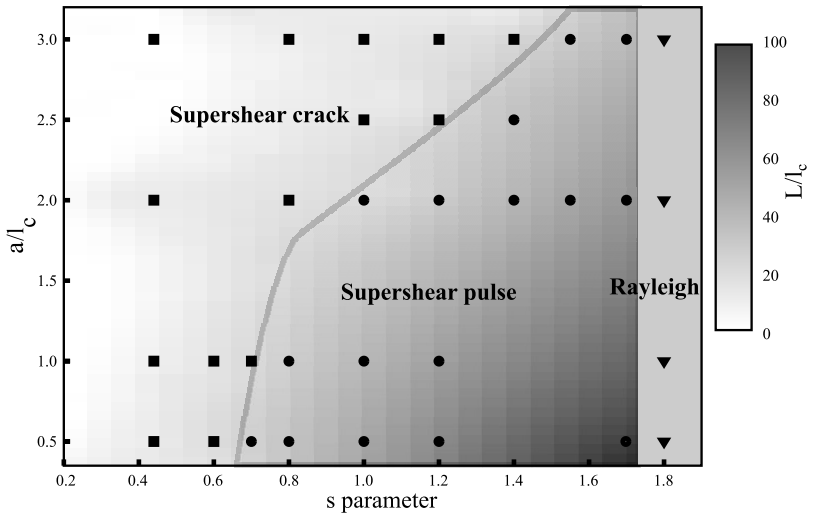

Figure 4. Supershear behavior as a function of the s parameter and the nucleation size a/l_c. The boundary between the crack regime and pulse regime follows an irregular path. The Rayleigh sub-shear propagation zone is also depicted. In a gray scale we qualitatively plot the distance L/l_c at which the supershear transition occurs.

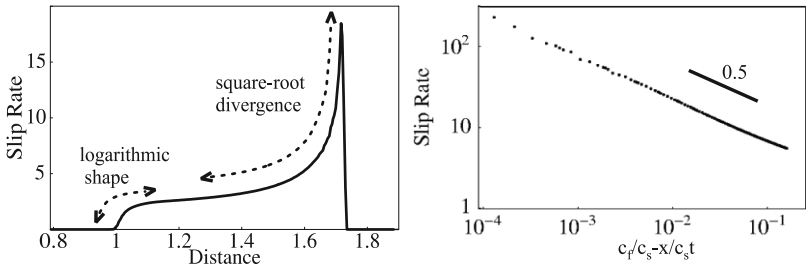

Figure 5. Arrest pulse solution. The arrest phase propagates at $c_h \approx c_s$, while the tip advances at c_f, close to c_p. The fit in a log-log plot shows a square-root divergence (indicated by the slope) in the neighborhood of the tip.

renormalized on a unique master curve and they show a square-root divergence at the slip rate tip and a logarithmic scaling in the vicinity of the arrest. Intersonic crack-like solutions are found for small s and large a/l_c with a spontaneous supershear transition, in which the rupture front remains glued to the interface Rayleigh wave. In both cases, the asymptotic solution is always a crack advancing at a velocity that tends to the P-wave speed. Acceleration records close to the fault show that most of the energy is carried by the shear Mach waves. In the pulse-like mode, an additional phase is linked to the secondary nucleation process.

[20] The transition between the two regimes is shown to be a non trivial function of both s and a/l_c. The travel distance, at which supershear transition occurs, strongly depends on the nucleation phase through the parameter a/l_c, for a given value of the strength parameter s. This implies a trade-off when interpreting such quantities based on seismological observations. Further analysis remains to be done to better quantify the role of the nucleation phase in the supershear transition in terms of time and travelling distance.

[21] **Acknowledgments.** This work has been supported by the EU training network SPICE, Seismic Wave Propagation and Imaging in Complex Media, and the ACI CATNAT of the French Ministry of Research. We gratefully thank P. Favreau, R. Madariaga, J.-P. Ampuero and two anonymous reviewers for their insightful comments.

References

Ampuero, J.-P., J.-P. Vilotte, and F. J. Snchez-Sesma (2002), Nucleation of rupture under slip dependent friction law: Simple models of fault zone, *J. Geophys. Res.*, *107*(B12), 2324, doi:10.1029/2001JB000452.

Andrews, D. J. (1976), Rupture velocity of plane strain shear cracks, *J. Geophys. Res.*, *81*, 5679–5687.

Andrews, D. J. (1985), Dynamic plane-strain shear rupture with a slip-weakening friction law calculated by a boundary integral method, *Bull. Seismol. Soc. Am.*, *75*(1), 1–21.

Bouchon, M., and M. Vallée (2003), Observation of long supershear rupture during the Ms = 8.1 Kunlunshan (Tibet) earthquake, *Science*, *301*, 824–826.

Broberg, K. B. (1978), On the transient sliding motion, *Geophys. J. R. Astron. Soc.*, *52*, 397–432.

Broberg, K. B. (1999), *Cracks and Fracture*, Elsevier, New York.

Burridge, R. (1973), Admissible speeds for plane-strain self-similar shear cracks with friction but lacking cohesion, *Geophys. J. R. Astron. Soc.*, *35*, 439–455.

Campillo, M., and I. R. Ionescu (1997), Initiation of antiplane shear instability under slip dependent friction, *J. Geophys. Res.*, *122*(B9), 20,363–20,371.

Dunham, E. M., and R. J. Archuleta (2004), Evidence for a supershear transient during the 2002 Denali fault earthquake, *Bull. Seismol. Soc. Am.*, *94*, 256–268.

Festa, G., and J. P. Vilotte (2005), The Newmark scheme as a velocity-stress time staggering: An efficient PML for Spectral Element simulations of elastodynamics, *Geophys. J. Int.*, *161*(3), 789–812, doi:10.1111/j.1365-246X.2005.02,601.x.

Freund, L. B. (1979), The mechanics of dynamic shear crack propagation, *J. Geophys. Res.*, *84*, 2199–2209.

Ida, Y. (1972), Cohesive force across the tip of a longitudinal-shear crack and Griffith's specific surface energy, *J. Geophys. Res.*, *77*, 3796–3805.

Jean, M. (1999), The non-smooth contact dynamics method, *Comput. Methods Appl. Mech. Eng.*, *177*, 235–257.

Komatitsch, D., and J. P. Vilotte (1998), The spectral element method: An efficient tool to simulate the seismic response of 2D and 3D geological structures, *Bull. Seismol. Soc. Am.*, *88*(2), 368–392.

Madariaga, R., and K. B. Olsen (2000), Criticality of rupture dynamics in 3-D, *Pure Appl. Geophys.*, *157*, 1981–2001.

Nielsen, S. B., and R. Madariaga (2003), On the self-healing fracture mode, *Bull. Seismol. Soc. Am.*, *93*(6), 2375–2388.

Obrezanova, O., and J. R. Willis (2003), Stability of intersonic shear crack propagation, *J. Mech. Phys. Solids*, *51*, 1957–1970.

Uenishi, K., and J. R. Rice (2003), Universal nucleation length for slip-weakening rupture instability under nonuniform fault loading, *J. Geophys. Res.*, *108*(B1), 2042, doi:10.1029/2001JB001681.

Xia, K. W., A. J. Rosakis, and H. Kanamori (2004), Laboratory earthquakes: The sub-Rayleigh-to-supershear rupture transition, *Science*, *303*, 859–861.

G. Festa and J.-P. Vilotte, Seismology Laboratory, Institut de Physique du Globe de Paris, 4 Place Jussieu, F-75252 Paris, France. (festa@ipgp.jussieu.fr)